Electronic structure of $BaPbO_3$ and Ba_2PbO_4

2008 J. Phys.: Condens. Matter 20 035219

(http://iopscience.iop.org/0953-8984/20/3/035219)

J. Phys.: Condens. Matter **20** (2008) 035219 (6pp) doi:10.1088/0953-8984/20/03/035219

Electronic structure of $BaPbO_3$ and Ba_2PbO_4

V R R Medicherla[1], **T Shripathi and N P Lalla**

UGC-DAE Consortium for Scientific Research, University Campus, Indore 452017, India

E-mail: ramarao@iopb.res.in

Received 8 October 2007, in final form 31 October 2007
Published 19 December 2007
Online at stacks.iop.org/JPhysCM/20/035219

Abstract

The electronic structure of $BaPbO_3$ and Ba_2PbO_4 was investigated using photoemission, x-ray diffraction (XRD) and tight binding linear muffin tin orbital (TB-LMTO) band structure techniques. $BaPbO_3$ is a base material for all Pb based superconductors. Rietveld analysis of the XRD data suggested that $BaPbO_3$ is an orthorhombically distorted perovskite with $Imma$ space group and Ba_2PbO_4 possesses tetragonal structure with $I4/mmm$ space group. LMTO calculations indicated an insulating ground state for Ba_2PbO_4 with a band gap of 1.3 eV and a metallic ground state for $BaPbO_3$. Ultraviolet photoemission results agree well with the LMTO calculations. The Pb–O1–Pb bond angle in the basal plane is a key parameter in deciding the electronic structure of these compounds. The Pb 4f and O 1s core levels of $BaPbO_3$ exhibited asymmetry on the high binding energy side of the peak, indicating that both Pb and O contribute to the density of states at the Fermi edge. The core levels of Ba_2PbO_4 did not exhibit asymmetry. Core level asymmetry can be used to probe the local density of states at E_F.

(Some figures in this article are in colour only in the electronic version)

1. Introduction

Barium metaplumbate $BaPbO_3$ (BPO) has attracted much attention due to its interesting physical properties. This simple perovskite has become the base material for several superconductors like $BaPb_{1-x}Bi_xO_3$ ($T_c \sim 12$ K) [1], $BaPb_{1-x}Sb_xO_3$ ($T_c \sim 3.5$ K) [2], and $BaPb_{1-x}Bi_{x/2}Sb_{x/2}O_3$ ($T_c \sim 6$ K) [3]. Orthorhombic perovskite, $BaPbO_3$, and body centered tetragonal perovskite, Ba_2PbO_4, are the end members of the interesting Ruddelsden–Popper series $Ba_{n+1}Pb_nO_{3n+1}$ [4]. Transport measurements exhibited metallic behavior in $BaPbO_3$ and a semiconducting behavior in Ba_2PbO_4 with temperature [5–7]. The driving mechanism of BPO metallicity is not very clear in the literature. It was attributed to oxygen vacancies by Ikushima and Hawalawa [8], and to unfilled d bands of Pb^{4+} by Shannon and Bierstedt [5]. BPO structure can be thought of as BaO layers separated by PbO_2 layers. Transport in BPO is mainly decided by the PbO_2 layer whereas the BaO layer contributes to the structural stability. Since the PbO_2 is metallic [9], the PbO_2 layer seems to be responsible for the metallic behavior of BPO. The PbO_2 layer in BPO is analogous to the Cu–O layer in YBCO superconductor. Another mechanism anticipated for BPO conduction is the partial substitution of Pb by Ba. This process would tend to produce some amount of Pb^{2+} and provides carrier generation [10].

The structure of $BaPbO_3$ has been studied extensively by several workers since its synthesis in 1958 by Hoppe and Blinne [11]. Earlier workers have reported a cubic perovskite structure for $BaPbO_3$ [11, 12]. But later workers reported that BPO ceramics are of orthorhombically distorted perovskite structure with space group $Pnma$ [5, 13]. Subsequent studies confirmed that $BaPbO_3$ is actually monoclinic at room temperature with $I2/m$ space group [14]. Recent structural investigations suggested that $BaPbO_3$ possesses orthorhombic structure with space group $Imma$ at room temperature [15, 3]. Upon cooling $BaPbO_3$, down to 15 K, it exhibited a structural transition from orthorhombic, $Imma$ structure to monoclinic, $C2/m$ structure [15]. On the other hand, investigations by Fu *et al* [16] did not evidence such a low temperature phase transition, but confirmed several structural phase transitions at higher temperatures.

The structure of $BaPbO_3$ is a complicated and long standing fundamental issue. The conduction mechanism also

[1] Present address: Institute of Physics, Sachivalaya Marg, Bhubaneswar, 751005, India.

seems to have diverse explanations. The structure of Ba_2PbO_4 on the other hand forms in the body centered tetragonal structure (K_2NiF_4 type) with $I4/mmm$ space group. Ba_2PbO_4 is a wide band gap semiconductor with a gap of 1.7 eV [17]. Band structure calculations suggested that the shortened apical Pb–O bond distance, compared to the planar Pb–O distance, plays a vital role in driving Ba_2PbO_4 semiconducting [4]. The actual mechanism driving Ba_2PbO_4 insulating is still not very clear.

$BaPbO_3$ has technological importance apart from possessing fundamentally challenging issues. This material demonstrates great potential in improving the characteristics of PZT films. BPO not only improves the microstructure, crystallinity, and ferroelectric properties but also reduces the leakage current of PZT films [18]. $BaPbO_3$ is also a useful material in applications such as ceramic electrodes, conductive pastes, anticorrosion pigments and sintered resistors [19].

This paper reports a study of the electronic structure of $BaPbO_3$ and Ba_2PbO_4 using XPS and UPS techniques along with TB-LMTO band structure calculations. As mentioned before, the structure of $BaPbO_3$ is controversial and may depend on the preparation method and conditions. Therefore, we have investigated the structure of these compounds using powder XRD and analyzed the data by the Rietveld refinement method. The output parameters of the Rietveld analysis were used for band structure calculations to obtain more relevant calculations on the materials prepared.

2. Experiment

Polycrystalline samples of $BaPbO_3$ and Ba_2PbO_4 were prepared by the solid state reaction method. High purity (99.99%) powders of $BaCO_3$ and PbO_2 were mixed in stoichiometric proportion and heated at 450 °C for 12 h to avoid the loss of Pb. The resulting mixture was calcined at 950 °C for 12 h. The mixture obtained was pressed into pellets and sintered in oxygen ambient at the calcination temperature for 24 h. During sintering, pellets were dipped in a powder of like composition to avoid the loss of volatile Pb at high temperatures. After a few cycles of this procedure, we obtained hard pellets of $BaPbO_3$ and Ba_2PbO_4.

Samples were characterized using the XRD technique. XRD measurements were carried out using a Rigaku make rotating anode x-ray generator (Rotoflex) with a Rigaku x-ray diffractometer. The powdered sample was pressed on a glass plate, mounted vertically on the sample table, and diffraction patterns were recorded using Cu Kα (1.54 Å) radiation. Data was collected in the 2θ range from 10° to 90° in steps of 0.02° using a scintillation detector. Only single-phase materials with no impurity phases were used in this study. XRD data was analyzed using the modified version of the profile refinement program of Young [20]. Various key parameters used in Rietveld refinement are atomic positions, occupancies and temperature factors and the instrument parameters like the zero angle and scale factor.

Photoemission measurements were carried out using a VSW ESCA machine equipped with a hemispherical analyzer, twin-anode x-ray source and a UV source. XPS and UPS measurements were done using Al Kα and He I radiations with resolutions of 0.9 eV and 0.1 eV respectively. The base pressure in the analysis chamber was maintained below 6.0×10^{-10} Torr. Freshly sintered pellets were loaded into the preparation chamber of the ESCA machine and were scraped repeatedly *in situ* in UHV with the help of a diamond file, until the O 1s signal did not exhibit further changes.

Electronic structure calculations were performed using the tight binding linear muffin tin orbitals (TB-LMTO) within the atomic sphere approximation (ASA) [21]. Calculations were done self-consistently and the combined correction terms were included. Spherical harmonics were included up to $l = 3$ (f-like orbital) in constructing basis functions. All the calculations were done within the allowed range of overlap between the atoms, enabling the use of the LMTO–ASA method. The structural parameters obtained by the Rietveld refinement of the XRD data were used as the input for these calculations.

Table 1. Structural parameters of $BaPbO_3$ and Ba_2PbO_4 obtained from the Rietveld analysis of the XRD patterns. Lattice parameters and bond lengths are given in Å.

Compound	$BaPbO_3$	Ba_2PbO_4
Structure	Orthorhombic	Tetragonal
Space group	$Imma$	$I4/mmm$
Lattice parameters	$a = 6.021$, $b = 8.501$, $c = 6.056$	$a = 4.284$ $c = 12.951$
Ba–O1	2.736	2.981
Ba–O2	2.853	2.419
Pb–O1	2.145	2.154
Pb–O2	2.149	2.061
Pb–O1–Pb	164.5°	180°
R_{wp} (%)	10.08	36.12
R_p (%)	7.05	26.12

3. Results

Figure 1 shows the observed and fitted data of the XRD patterns obtained for $BaPbO_3$ and Ba_2PbO_4. XRD data for $BaPbO_3$ was excellently fitted with the space group $Imma$ and could not be fitted to the space group $Pbnm$ as reported earlier [5]. The Ba_2PbO_4 data was nicely fitted using the $I4/mmm$ space group [4].

Various bond lengths, bond angles and R-factors obtained from the Rietveld fitting of the XRD data are shown in table 1. The lattice parameters obtained are in good agreement with the previously reported data [15, 5]. The orthorhombic distortion observed in $BaPbO_3$ (space group $Imma$) is quite uncommon in perovskite oxides. Similar distortion has previously been reported for $PrAlO_3$ [22]. It is interesting to note that the lattice parameters a and c differ only from the second decimal place onwards and the Pb–O1 and Pb–O2 bond lengths are also of similar magnitude in $BaPbO_3$ (table 1). In Ba_2PbO_4, the Pb–O2 bond length is smaller than the Pb–O1 bond length which is an unusual distortion in layered oxides. The Pb–O1–Pb bond angle increases from 164.5° in $BaPbO_3$ to 180° in Ba_2PbO_4.

Figure 2 shows the experimental valence band spectra of $BaPbO_3$ and Ba_2PbO_4 excited using He I radiation and compared with the calculated DOS. The experimental valence

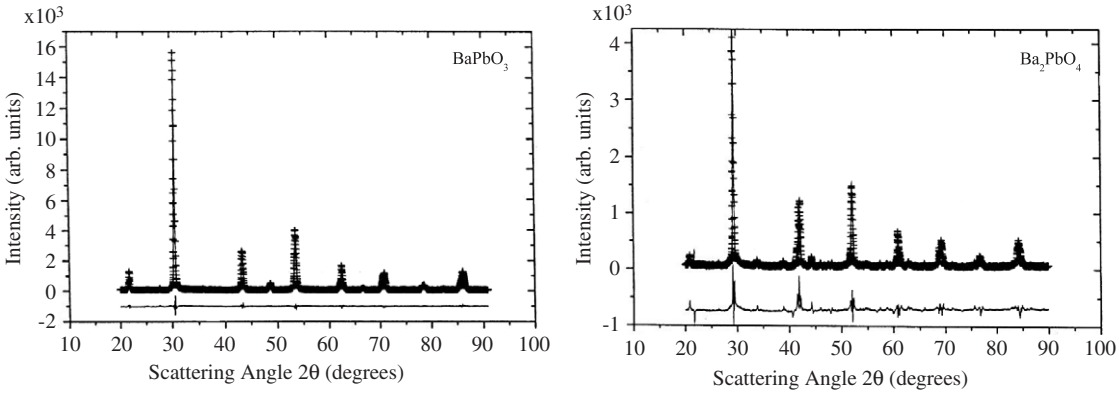

Figure 1. Observed (+) and fitted (——) x-ray diffraction patterns of $BaPbO_3$ (left panel) and Ba_2PbO_4 (right panel). The difference between the observed and fitted patterns is shown at the bottom.

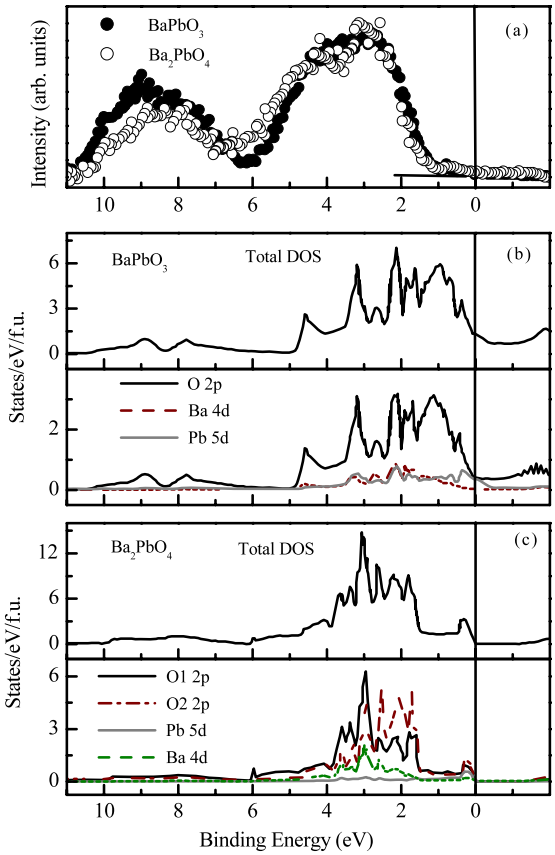

Figure 2. (a) Experimental valence band spectra of $BaPbO_3$ (●) and Ba_2PbO_4 (○) excited by He I radiation. (b) Calculated total DOS and partial DOS (O 2p, Ba 4d and Pb 5d) of $BaPbO_3$. (c) Calculated total DOS and partial DOS (O1 2p, O2 2p, Pb 5d and Ba 4d) of Ba_2PbO_4.

bands (figure 2(a)) of the two the compounds appear similar, exhibiting two prominent features of 11–6 and 6–1 eV binding energies. The intensity close to the Fermi edge appears to be zero or very small. The intensity of the feature around 9 eV is a little higher in $BaPbO_3$ compared to Ba_2PbO_4. The calculated DOS of $BaPbO_3$ showed a small number of states for 11–5 eV and a strong contribution between 5 eV and the Fermi edge, and exhibits a finite DOS at E_F indicating the metallic nature. Comparing the total DOS with the partial DOS of O 2p, Pb 5d and Ba 4d (lower panel of figure 2(b)), it is evident that the total DOS has its primary contribution from O 2p with small contributions from Pb 5d and Ba 4d states. States in the vicinity of the Fermi edge arise only from Pb 5d and O 2p. Contributions from Pb 6s and Ba 5p (not shown) states are insignificant in this energy range. The calculated total DOS of Ba_2PbO_4 (figure 2(c)) is similar to that of $BaPbO_3$ below the Fermi edge. Unlike $BaPbO_3$, Ba_2PbO_4 exhibits a gap of 1.3 eV starting at the Fermi edge, suggesting a semiconducting nature of this compound. The partial DOS of various atoms of Ba_2PbO_4 are shown in the lower panel of figure 2(c). Since Ba_2PbO_4 is a layered compound, the O1 and O2 2p DOS are shown separately. Major contributions to the total DOS arise from O 2p (both O1 and O2) states and a small contribution comes from Ba 4d and Pb 5d states. O2 2p has more states closer to the Fermi edge (around 2 eV B.E.), whereas O1 2p has a higher contribution at 3.0 eV B.E. Such a difference in the distribution of states of O1 and O2 may be related to the shorter Pb–O2 bond length compared to the Pb–O1 bond length obtained by the Rietveld analysis of the XRD data (see table 1). The relative intensities of the calculated total DOS for both $BaPbO_3$ and Ba_2PbO_4 are significantly different from the experimental results, presumably due to the fact that experimental spectra are influenced by the matrix element effects and lifetime broadening of the holes and electrons in addition to various other final state effects which are not considered in the *ab initio* calculations. Agreement between the experimental and calculated results is better in the case of Ba_2PbO_4 compared to that of $BaPbO_3$.

High resolution valence band spectra in the vicinity of the Fermi edge excited by He I radiation are shown in figure 3. There is a striking difference between the spectra of $BaPbO_3$ and Ba_2PbO_4 near the Fermi edge. $BaPbO_3$ exhibits finite intensity at the Fermi edge, whereas Ba_2PbO_4 exhibits zero intensity. This observation is in agreement with the metallic and semiconducting behaviors observed respectively for $BaPbO_3$ and Ba_2PbO_4 in our calculated results. Intensity at the Fermi edge in $BaPbO_3$ is contributed by O 2p and Pb 5d states as seen in figure 2(b).

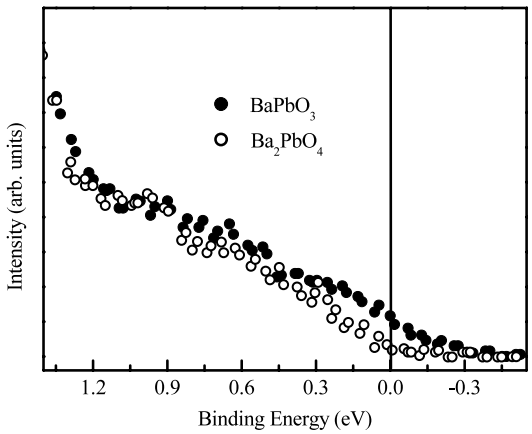

Figure 3. Valence band spectra near the Fermi edge for $BaPbO_3$ (●) and Ba_2PbO_4 (○) excited by He I radiation.

Core levels were analyzed using the asymmetric Gaussian–Lorentzian (AGL) sum function [23] defined as

$$\mathrm{AGL}(x, p, w, h, m, TS, TL) = h\left\{(1-m)\mathrm{e}^{-Q\ln 2} + \frac{m}{1+Q} + TS(1-\mathrm{e}^{-Q\ln 2})\mathrm{e}^{\frac{-6.9}{TL}Q}\right\} \quad (1)$$

where $Q = [\frac{2(x-p)}{w}]^2$; p, the peak position; w, the FWHM of the peak; h, the integrated area of the peak; m, the GL mixing parameter (0 for 100% Gaussian and 1 for 100% Lorentzian); TS and TL are the parameters for the asymmetric tail and are functions of m, w ($TS = 0$ for a symmetric GL function).

Ba 3d and Pb 4f core level spectra of $BaPbO_3$ and Ba_2PbO_4 are shown in figure 4. Ba 3d spectra of the two compounds look similar and overlap with each other. These spectra were fitted using the asymmetric Gaussian–Lorentzian sum function (equation (1)). Ba 3d spectra were fitted with a FWHM of 3.6 eV, spin–orbit splitting (S.O.S.) of 15.4 eV and TS of 0 (no asymmetry). Pb 4f spectra of the two compounds are compared in figure 4(b). Interestingly, $BaPbO_3$ exhibits more asymmetry compared to Ba_2PbO_4. As shown in the graph, Pb 4f spectra of Ba_2PbO_4 could be fitted very well by using equation (1) with $TS = 0$ (no asymmetry). On the other hand the Pb 4f spectrum of $BaPbO_3$ was fitted using equation (1) with $TS = 0.35$ and $TL = 15$ (figure 4(c)).

Figure 5 shows the O 1s spectra of Ba_2PbO_4 and $BaPbO_3$. Ba_2PbO_4 exhibits a high B.E. shoulder at 530.9 eV along with the main peak at 528.9 eV. These peaks were deconvoluted using equation (1) without the asymmetry part ($TS = 0$) and the FWHM values obtained are 2.8 eV for the high B.E. shoulder and 1.9 eV for the main peak. Interestingly, the O 1s spectrum of $BaPbO_3$ is a single peak with high asymmetry and could not be fitted with $TS = 0$. The AGL fit resulted in $TS = 0.75$, $TL = 35$ with a FWHM of 1.95 eV for the O 1s spectrum of $BaPbO_3$. The asymmetric O 1s line shape for $BaPbO_3$ was previously reported by Wertheim *et al* [24]. The double-peak structure of the O 1s core level in Ba_2PbO_4 is due to the layered nature of the compound. The structure of Ba_2PbO_4 can be regarded as a stacking of single $BaPbO_3$ layers separated by BaO layers [25]. The main peak corresponds to

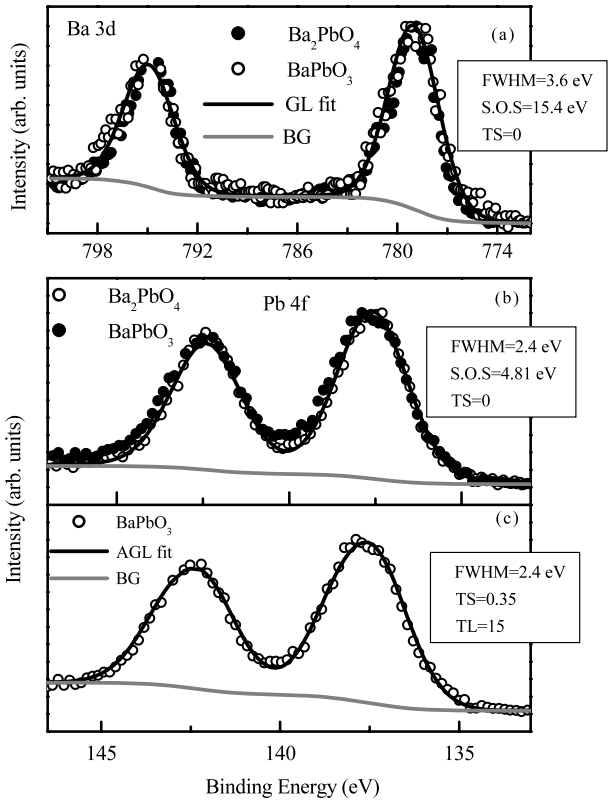

Figure 4. (a) Ba 3d spectra along with the AGL fit (——) to the data for $BaPbO_3$ (○) and Ba_2PbO_4 (●). (b) Pb 4f spectra of $BaPbO_3$ (●) and Ba_2PbO_4 (○) along with the AGL fit (——) to the Ba_2PbO_4 data. (c) Pb 4f data of $BaPbO_3$ (○) along with the AGL fit (——). BG represents the Shirley background.

the oxygen in the $BaPbO_3$ layer and the shoulder corresponds to oxygen in the BaO layer. The FWHM of the shoulder is much higher compared to that of the main peak for Ba_2PbO_4, which can be attributed to the presence of little inter-grain oxygen contributing to the O 1s signal around the same energy. The main peaks for both the compounds occur at 528.9 eV.

4. Discussion

The structure of $BaPbO_3$ has extensively been studied in the past by several workers and was controversial for many years. XRD data of $BaPbO_3$ prepared in this study using the solid state reaction method could be fitted well to the space group $Imma$ and the result is in agreement with the recently reported structure of $BaPbO_3$ [15, 16]. Structural data of Ba_2PbO_4 was fitted to the $I4/mmm$ space group which agrees well with the earlier reports [4].

UPS results close to the Fermi edge indicated an insulating nature for Ba_2PbO_4 and a metallic nature for $BaPbO_3$. Our LMTO calculations supported the results from UPS by exhibiting finite states at E_F for $BaPbO_3$ and a gap of about 1.3 eV for Ba_2PbO_4. The band gap obtained in our calculations is similar in magnitude to the gap observed by Matheiss [4]. The electronic properties of these materials are primarily decided by the overlap of Pb 5d6s states with O 2p states. The opening up of a gap in Ba_2PbO_4 is related to the unusual

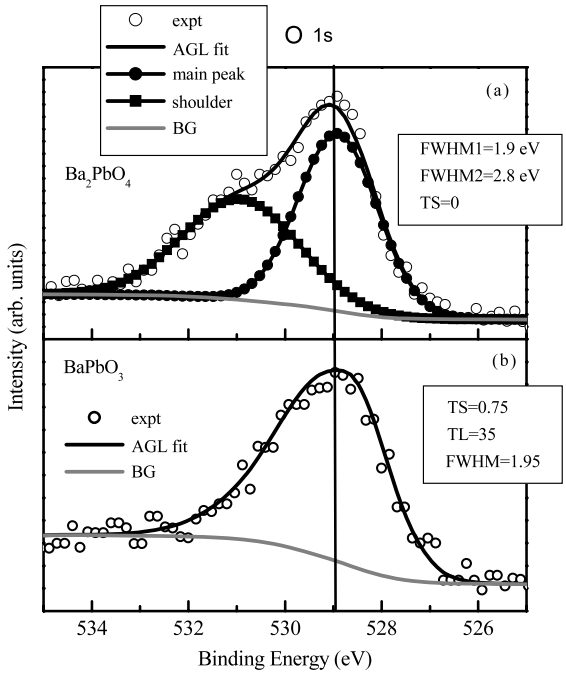

Figure 5. O 1s spectra of (a) Ba_2PbO_4 (○) with the AGL fit (——) and (b) $BaPbO_3$ (○) with the AGL fit (——). BG represents the Shirley background.

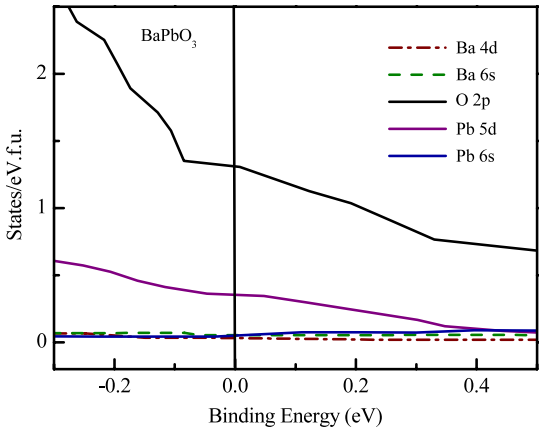

Figure 6. Angular momentum projected DOS of Ba, Pb and O in $BaPbO_3$ in the vicinity of the Fermi edge.

distortion of the PbO_6 octahedra with smaller apical Pb–O2 bond length and larger planar Pb–O1 bond length (table 1) as obtained from our Rietveld analysis of the XRD data. Interestingly, the apical Pb–O2 bond length in Ba_2PbO_4 is smaller than the planar Pb–O1 bond length in $BaPbO_3$ which implies that Ba_2PbO_4 should also be conducting. But the conduction predominantly occurs in the basal plane and thus only the planar bond length (Pb–O1) plays a crucial role in deciding the electronic properties. Pb–O1 bond lengths are almost the same in magnitude (table 1) for $BaPbO_3$ and Ba_2PbO_4 and the opening up of a gap in Ba_2PbO_4 cannot be explained by considering the Pb–O1 bond length. The Pb–O1–Pb bond angle can influence the integral of overlap between Pb 5d6s and O 2p states. Our structural studies indicated that the Pb–O1–Pb bond angle increases from 164.5° in $BaPbO_3$ to 180° in Ba_2PbO_4. Straightening of the bond in Ba_2PbO_4 can reduce the overlap of Pb and O states and thus can induce a gap.

The core levels of Ba_2PbO_4 did not exhibit asymmetry and, interestingly, asymmetry was not observed in the Ba 3d core level of $BaPbO_3$ either. The Pb 4f and O 1s core levels of $BaPbO_3$ exhibited asymmetry. Asymmetry in the core levels has been observed for metals with high density of states at the Fermi level [26]. Core level shape can be asymmetric in semi-metals also [27, 28]. Asymmetry is mainly due to the influence of the core hole potential on the DOS in the vicinity of the Fermi edge. Asymmetry of a core level in an atom depends on the local DOS at E_F corresponding to that atom [29]. In the case of Ba_2PbO_4, both UPS and LMTO studies exhibited no states at E_F and thus the core levels exhibited no asymmetry. On the other hand, $BaPbO_3$ shows finite states at E_F in both UPS and LMTO studies. Interestingly, only Pb 4f and O 1s core levels of $BaPbO_3$ exhibited asymmetry whereas the Ba 3d spectrum did not exhibit asymmetry.

To understand the origin of asymmetry in Pb 4f and O 1s spectra in comparison to Ba 3d spectrum of $BaPbO_3$, we have shown the Ba (4d, 6s), O 2p, Pb (6s, 5d) angular momentum projected DOS in figure 6. The total DOS were primarily contributed by these levels in $BaPbO_3$. O 2p has the highest DOS at E_F compared to other levels and thus the most asymmetric O 1s core level with $TS = 0.75$ and $TL = 35$ was observed. Pb also contributes to the total DOS through considerable 5d and a small number of 6s states, but the Pb contribution is significantly low compared to the O contribution to the total DOS at E_F. Therefore, the asymmetry observed in the Pb 4f spectrum is very small with the $TS = 0.35$ and $TL = 15$ compared to the asymmetry in O 1s. The contribution made by Ba to the total DOS of $BaPbO_3$ is extremely small or zero and thus Ba 3d did not exhibit asymmetry in $BaPbO_3$. Core level asymmetry can be used to probe the local DOS at E_F.

5. Conclusion

We have investigated the electronic structure of $BaPbO_3$ and Ba_2PbO_4 using photoemission and TB-LMTO methods. Valence bands obtained from UPS measurements were interpreted using the *ab initio* TB-LMTO calculations. The XRD data was analyzed using the Rietveld refinement method. Our investigations showed an insulating ground state for Ba_2PbO_4 and a metallic ground state for $BaPbO_3$. The Pb–O1–Pb bond angle plays a key role in opening up a gap in Ba_2PbO_4. Core level asymmetries observed in Pb 4f and O 1s spectra of $BaPbO_3$ are related to the local DOS of Pb 5d6s and O 2p states, respectively, at the Fermi edge.

References

[1] Sleight A W, Gillson J L and Bierstedt P E 1975 *Solid State Commun.* **17** 27
[2] Cava R J *et al* 1989 *Nature* **339** 291
[3] Fu W T and Drost R J 1998 *Physica* C **304** 51

[4] Matheiss L F 1989 *Phys. Rev.* B **42** 359
[5] Shannon R D and Bierstedt P E 1970 *J. Am. Ceram. Soc.* **53** 635
[6] Cava R J, Takagi H, Krawjewski J J, Peck W F Jr and Hwang H Y 1993 *Phys. Rev.* B **47** 11525
[7] Verheijen A A, Fu W T, Ruitenbeek J M, Smits A, Xu Q and De Jongh L J 1989 *Solid State Commun.* **71** 573
[8] Ikushima H and Hawakawa S 1966 *Solid-State Electrochem.* **9** 921
[9] Samsonov G V 1973 *The Oxide Handbook* (New York: IFI/Plenum) p 222
[10] Heish Y-H and Fu S-L 1992 *Ceram. Int.* **18** 289
[11] Hoppe R and Blinne K 1958 *Z. Anorg. Allg. Chem.* **293** 251
[12] Wagner G and Binder H 1959 *Z. Anorg. Allg. Chem.* **298** 12
Weiss R 1958 *C. R. Acad. Sci.* **246** 3073
Nitta T, Ngase K, Hayakawa S and Iida Y 1965 *J. Am. Ceram. Soc.* **48** 642
[13] Shuvaeva E T and Fesenko E G 1970 *Kristallografiya* **15** 379
Thornton G and Jacobson A J 1976 *Mater. Res. Bull.* **11** 837
Cox D E and Sleight A W 1977 *ERDA Energy Res. Abstr.* **2** 7623
[14] Marx D T, Padaelli P G, Jorgensen J D, Hitterman R L, Hinks D G, Pei S and Dabrowski B 1992 *Phys. Rev.* B **46** 11444
Ritter J, Ihringery K J, Maichle W, Prandly A, Hoser A and Hewat Z 1989 *Physik* B **75** 297
[15] Moussa S M, Kennedy B J and Vogt T 2001 *Solid State Commun.* **119** 549
[16] Fu W T, Visser D and Ijdo D J W 2005 *Solid State Commun.* **134** 647
Fu W T, Visser D, Knight K S and Ijdo D W J 2007 *J. Solid State Chem.* **180** 1559
[17] Xu Q, Fu W T, van Ruitenbeek J M and de jongh D J 1990 *Physica* C **167** 271
Rosseinsky M J and Prassides K 1991 *Acta Crystallogr.* C **47** 2519
[18] Liang C-S, Lee Y-S and Wu J-M 2005 *J. Cryst. Growth* **283** 390
Liang C-S, Wu J-M and Chang M-C 2002 *Appl. Phys. Lett.* **81** 3624
Lou Y-R and Wu J-M 2001 *Appl. Phys. Lett.* **79** 3669
[19] Kuwabara M 1989 *J. Mater. Sci. Lett.* **8** 411
Nomura S 1985 *Japan. J. Appl. Phys.* **24** 736
Nitta T, Taki H and Nagase K 1964 *Japan. J. Appl. Phys.* **17** 3
[20] Young R A 1995 *The Rietveld Method* (Oxford: Oxford University Press)
[21] Anderson O K 1975 *Phys. Rev.* B **12** 3060
[22] Burbank R P 1970 *J. Appl. Crystallogr.* **3** 112
[23] Seah M P and Brown M T 1998 *J. Electron Spectrosc. Relat. Phenom.* **95** 71
Zhang B, Quan Z, Zhang T, Guo T and Mo S 2001 *J. Appl. Phys.* **101** 014107
[24] Wertheim G K, Remeika J P and Buchanan D N E 1982 *Phys. Rev.* B **26** 2120
[25] Jacob K T and Jayadevan K P 1998 *Mater. Sci. Eng.* B **52** 134
[26] Doniach S and Sunjic M 1970 *J. Phys. C: Solid State Phys.* **3** 285
[27] van Attekum P M Th M and Wertheim G K 1979 *Phys. Rev. Lett.* **43** 1896
[28] Rama Rao M V and Shripathi T 1996 *J. Electron Spectrosc. Relat. Phenom.* **78** 159
[29] Shevchick N J 1974 *Phys. Rev. Lett.* **33** 1336